**FULL PAPER**

# Ultra-small CuO nanoparticles with tailored energy-band diagram synthesized by a hybrid plasma-liquid process

**Tamilselvan Velusamy[1]** | **Anna Liguori[2]** | **Manuel Macias-Montero[1]** |
**Dilli Babu Padmanaban[1]** | **Darragh Carolan[1]** | **Matteo Gherardi[2,3]** |
**Vittorio Colombo[2,3]** | **Paul Maguire[1]** | **Vladimir Svrcek[4]** | **Davide Mariotti[1]**

[1] Nanotechnology and Integrated Bio-Engineering Centre (NIBEC), Ulster University, Newtownabbey, United Kingdom

[2] Advanced Mechanics and Materials, Interdepartmental Center for Industrial Research (AMM-ICIR), Alma Mater Studiorum—Università di Bologna, Bologna, Italy

[3] Department of Industrial Engineering (DIN), Alma Mater Studiorum—Università di Bologna, Bologna, Italy

[4] Department of Energy and Environment, Research Center of Photovoltaics, National Institute of Advanced Industrial Science and Technology (AIST), Tsukuba, Japan

**Correspondence**
Tamilselvan Velusamy and Davide Mariotti, Nanotechnology and Integrated Bio-Engineering Centre (NIBEC), Ulster University, Newtownabbey, UK.
Email: tamila.nt@gmail.com (T.V.); d.mariotti@ulster.ac.uk (D.M.)

CuO is a versatile p-type material for energy applications capable of imparting diverse functionalities by manipulating its band-energy diagram. We present ultra-small quantum confined cupric oxide nanoparticles (CuO NPs) synthesized via a simple one-step environmentally friendly atmospheric pressure microplasma synthesis process. The proposed method, based on the use of a hybrid plasma-liquid cell, enables the synthesis of CuO NPs directly from solid metal copper in ethanol with neither surfactants nor reducing agents. CuO NPs films are then used for the first time in all-inorganic third generation solar cell devices demonstrating highly effective functionalities as blocking layer.
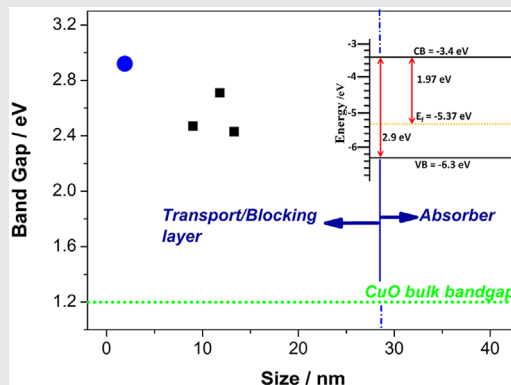


**KEYWORDS**
band structure, cupric oxide quantum dots, one step-green synthesis, quantum dots/inorganic solar cells

## 1 | INTRODUCTION

Transition metal oxides, due to their inertness, stability, raw material abundance, and low-cost, are highly desirable materials for many applications, for example, solar cells, supercapacitors, light emitting diodes, photodetectors, field effect transistors, batteries and bio and gas sensors, among others.[1–10] Furthermore, as with other materials, at the nanoscale, metal-oxides can present interesting, important and tunable size-dependent optoelectronic properties.[7,11,12] Metal-oxides are generally characterized by very wide bandgaps, whereas CuO is a p-type low bandgap (~1.2 eV in bulk form) and non-toxic

material.[13–18] The possibility of manipulating the CuO bandgap, through quantum confinement, from 1.2 (bulk) to >2 eV[13,16–22] is an exciting opportunity as it would make CuO a highly versatile and attractive material for a range of applications; for instance, it would be possible to use CuO nanoparticles with tunable properties as absorber or transport/blocking layers in photovoltaic devices.

Various physical, chemical, and physicochemical techniques have been employed for synthesizing CuO nanostructures with varying size and shape.[16,18,20,23,24] However, these techniques suffer from numerous disadvantages including complex and time consuming steps, high temperatures, inert

atmosphere, expensive source materials, toxic organic solvents, and surfactants.[23,25,26] Furthermore, the control of the resulting morphology, crystallinity, and agglomeration of the nanostructures is a significant challenge which demands additional cleaning steps to remove undesired by-products and chemical impurities or residues.[23,26–29] The presence of surfactant or ligand chemistries is essential for minimizing particle coalescence and agglomeration during standard colloid synthesis; however, such chemistries impact significantly on the resultant nanoparticle optoelectronic properties and restrict the opportunity for bandgap tuning.[27] Synthesis of non-agglomerated and pure CuO nanostructures is imperative for their successful integration in application devices,[29,30] and therefore, developing an alternative, cheap, and environmentally friendly synthesis method is highly desirable.

We report for the first time, the synthesis of pure colloidal CuO nanoparticles, without surfactant or ligand chemistries, which is essential to maintain important opto-electronic functionalities.[29,30] We demonstrate a stable one-step plasma-liquid hybrid process for the synthesis of fully dispersed and non-agglomerated ultra-small quantum confined CuO nanoparticles (NPs) from bulk copper electrodes in ethanol. Hybrid plasma-liquid methods are an emerging class of synthesis techniques that have been attracting great interest due to their simplicity and ability to produce quickly and at low cost a very wide range of materials including metallic, bimetallic, semiconducting, and metal-oxide colloidal nanoparticles from simple and environmentally friendly precursors.[28,31–34] It is believed that highly reactive and transient chemistries produced by plasma-liquid interactions, coupled with local charging of the synthesized NPs, lead to the generation of previously inaccessible surface chemistries and electrostatic colloidal stabilization. After the synthesis process, a detailed physical and chemical characterization of the produced nanoparticles was carried out, which confirmed the characteristic crystal structure and chemical composition of CuO. Widening of the bandgap induced by the quantum confinement has been clearly observed. As a further step, the *energy-band diagram* (EBD) was evaluated in order to envision the functional role of these CuO NPs for application devices. It was observed that quantum confinement shifts the conduction band edge to lower energy absolute values making CuO NPs ideal as an electron blocking layer. This is particular beneficial for a range of devices with absorbers that have relatively low conduction band edges (in absolute values) and for instance for cells optimized to the ultra-violet region (e.g., in multi-junction devices).

In order to demonstrate CuO NPs functionality, we have incorporated CuO NPs layers into third generation all-inorganic photovoltaic devices, with potential for application in very low-cost and environmentally friendly devices including multi-junction architectures. The full device structure includes quantum confined silicon nanocrystals (Si NCs) as the active layer, a $TiO_2$ hole blocking layer and indium-tin oxide/gold contacts. Devices were fabricated at atmospheric pressure utilizing all-inorganic, abundant, "green," and non-toxic materials and designed to provide suitable band energy alignment. These third generation devices were, therefore, used to demonstrate the ability of the CuO NPs to provide an effective barrier to electrons produced in the Si NCs avoiding interface recombination. While quantum confinement has been used for bandgap engineering and to provide suitable absorption matching of the solar energy, here we highlight for the first time the additional potential of quantum confinement as a means to tailor the full EBD, leading to EBD- and band alignment-engineering, across all layers of the device structure.

## 2 | EXPERIMENTAL SECTION

For the synthesis of CuO NPs, we employed here an atmospheric pressure direct-current (DC) microplasma (Figure 1a) generated between a Ni tube and 5 mL of ethanol (Sigma-Aldrich, Ethyl alcohol, pure 200 proof, for molecular biology). A copper (Cu) foil (Fisher Scientific, product code: 10685292, 0.1 mm thickness), immersed by 5 mm in ethanol, is used as anode and is placed at about 3 cm from the Ni tube (0.7 mm internal diameter, 1 mm outer diameter), which acts as cathode. The distance between the Ni tube and the liquid surface is initially adjusted at 1 mm. Pure He is flown through the Ni tube and its mass flow rate is kept constant at 50 standard cubic centimeters per minute (sccm). The voltage, applied to the Cu foil with the Ni tube grounded through a 100 kΩ ballast resistor, is initially set at 3 kV until the current reaches 0.5 mA. The current value is maintained constant throughout the whole process by progressively lowering the voltage from 3 kV to around 2 kV. This was necessary because the solution conductivity varies as the process generates ions, in part also due to water vapor absorbed in the solution from air.[35–37] The synthesis is initiated as soon as the microplasma is generated and the presence of NPs is clearly visible at naked eye after a few minutes due to the solution turning yellow; for consistency, the results reported here will relate to CuO NPs produced for a total of 30 min in 10 min consecutive processing steps. Figure 1b reports photos of the solution after (I) 10 min, (II) 20 min, and (III) 30 min processing clearly showing the change of the color of the solution turning into a colloid during the synthesis process (see Supporting information [SI] Figure S1).

## 3 | RESULTS AND DISCUSSION

Following the synthesis, the CuO NPs have been characterized without any post-synthesis treatment. The synthesis of
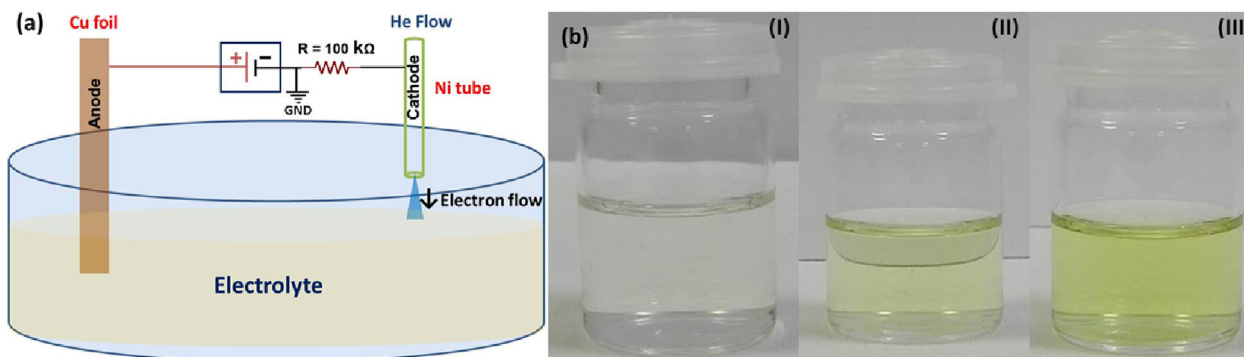
**FIGURE 1** (a) Schematic diagram of the direct current microplasma setup used for the synthesis of CuO nanoparticles. (b) Photographs of the processed samples after (I) 10 min, (II) 20 min, and (III) 30 min processing

NPs was confirmed by transmission electron microscopy (TEM; JEOL JEM-2100F); samples for TEM analysis were drop-casted on carbon coated Au grids. Figure 2a shows a low magnification image, which exhibits the presence of non-agglomerated NPs; analysis of hundreds of NPs has indicated the presence of spherical particles with a diameter distribution that is closely fitted with a log-normal distribution (1.9 nm arithmetic mean and $\pm$0.49 nm variance) (Figure 2b).

The crystal structure was also determined by transmission electron microscopy (TEM). High resolution TEM (HRTEM) image of the CuO NPs are shown in Figure 2c. Figure 2c clearly highlights the existence of atomic fringes indicating a crystalline structure. The d-spacing, determined by fast Fourier transform (FFT) was within 0.20–0.21 nm (e.g., see Figure 2c.I,II), which corresponds to the CuO (201) and CuO (012) plane.[38,39] Also, corresponding selected area electron diffraction pattern (SAED) is displayed in Figure S2 in Supporting Information. X-ray diffraction (XRD, Bruker D8 Discover) was carried out for CuO NPs film and it is presented in Supporting Information (see Figure S2).

The chemical composition was assessed by X-ray photoelectron spectroscopy (XPS) with an Axis Ultra DLD spectrometer (Kratos Analytical, Japan) with monochromated Al $K\alpha$ X-rays source and by Fourier transform infrared

spectroscopy (FTIR, Thermo Scientific, Nicolet iS5, 4 cm$^{-1}$, resolution, totally scanned it for 50 times in N$_2$ atmosphere). Sample preparation for XPS was carried out by drop-casting the colloids on molybdenum foil and dried.

FTIR analysis was carried out from as-prepared colloids, which were spray-coated and dried on a silicon wafer. Figure 3a reports the FTIR spectrum of the spray-coated CuO NPs onto Si wafer and details the assignment of the corresponding peaks. The absorption peaks from 420 to 700 cm$^{-1}$ belong to the CuO.[13,16,18] In particular, the peaks at 428, 503, and 536 cm$^{-1}$ are characteristic stretching vibrations of Cu—O on monoclinic CuO.[16,19,20,40] The absorption at 447 cm$^{-1}$ represents the stretching mode of Cu—O[40] and the absorption at 485 cm$^{-1}$ is due to the Cu—O stretching along [101] direction.[21] Furthermore, the absence of the infrared-active modes at 610 cm$^{-1}$ from the Cu$_2$O phase confirms the purity of the CuO phase.[19] Relevant high resolution XPS spectra of the NPs is displayed in Figure 3b (see Figure S3a in the Supporting Information for the survey scan spectrum). The Cu 2p core level binding energies at 934.8 and 954.7 eV are attributed to the Cu 2p$_{3/2}$ and Cu 2p$_{1/2}$, respectively.[41,42] Additional sub peak at 941.8 eV also attributed from the Cu$^{2+}$ state.[43]
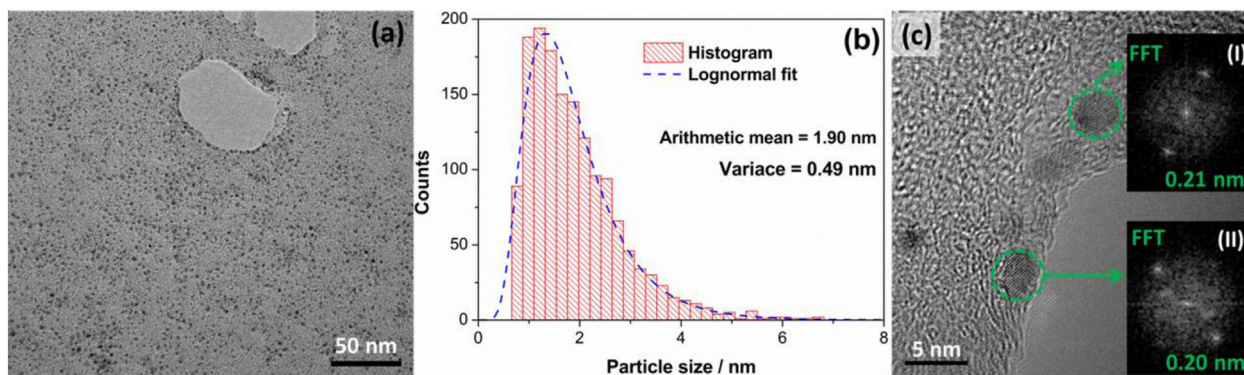


**FIGURE 2** (a) Low magnification transmission electron microscopy image of CuO nanoparticles and (b) corresponding diameter distribution with resulting arithmetic mean and variance. (c) High resolution transmission electron microscopy image of the CuO nanoparticles and corresponding fast Fourier transform (FFT) images (insets I and II)
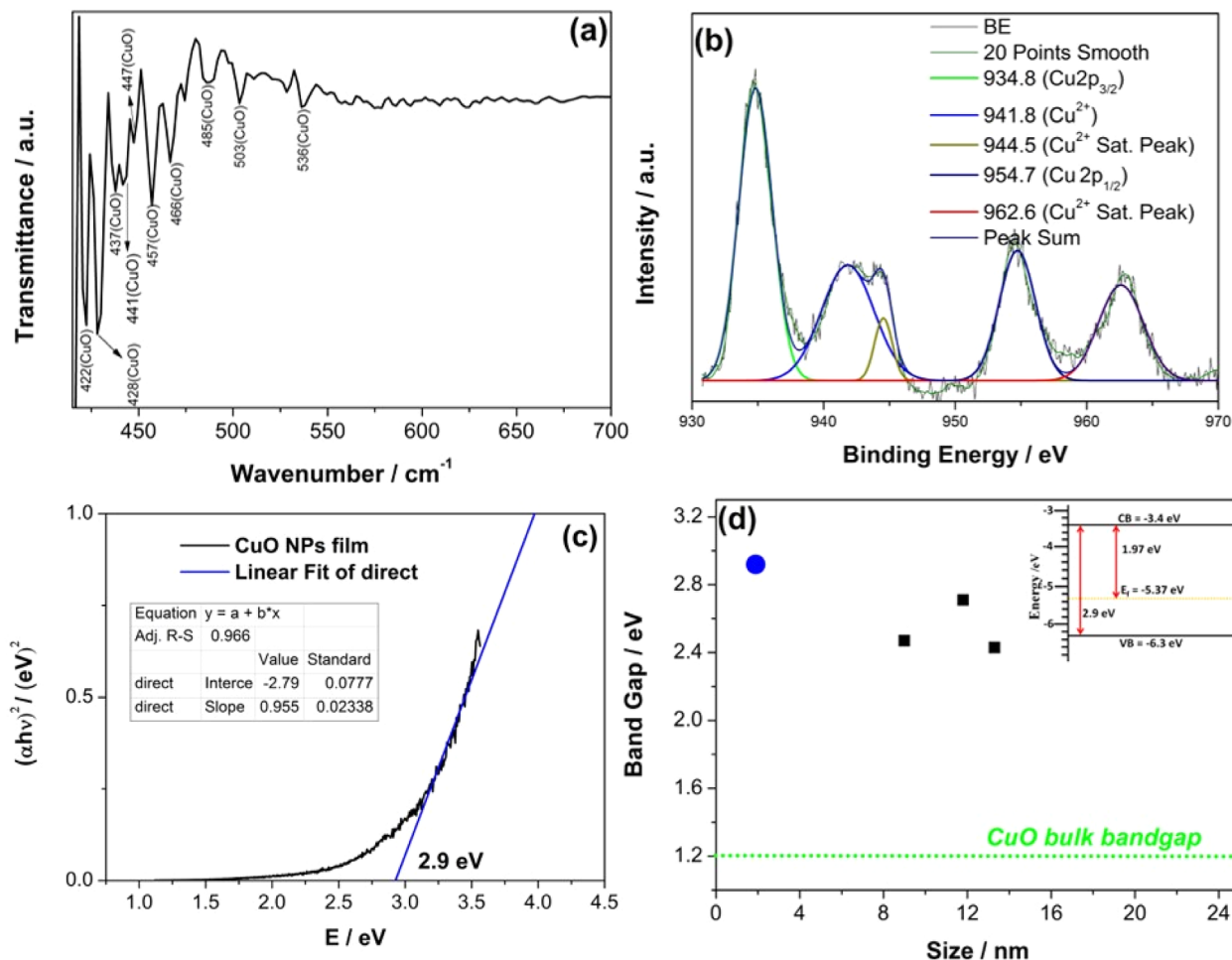
**FIGURE 3** (a) Fourier transform infrared spectrum of spray-coated CuO nanoparticles (NPs). (b) X-ray photoelectron spectra of Cu 2p core level for CuO NPs. (c) Tauc plot for the spray coated CuO NPs. (d) Bandgap of different CuO nanostructures versus their sizes; bandgap values (black squares) are taken from the literature and compared with the results of this work (blue dot); the value of the bulk bandgap is also provided (1.2 eV, dotted green line).[13,16] The inset image reports the band energy diagram of CuO NPs, which is determined from its measured bandgap, valence band, and Fermi level values
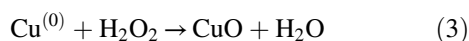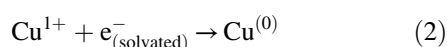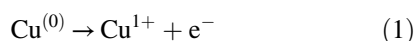
Additionally, the presence of the satellite peaks (from 940 to 946 eV and 960 to 965 eV) on the higher binding energy side of the Cu 2p main peaks confirms the formation of pure CuO phase.[19,41,44,45] CuO exhibits an unfilled $d^9$ configuration in its divalent state, wherein Cu contributes a d-electron from its completed d-shell for bonding with oxygen; on the contrary, $Cu_2O$ would show a filled $d^{10}$ configuration in ground state. Creation of a core hole during the photoemission process is favored for the charge transition from the surrounded ligands ($O^{2-}$ ions) into unfilled $d^9$ valance state of the $Cu^{2+}$ ions. This charge transfer results in the main peak (in lower binding energy) with $d^{10}L^{-1}$ character (L represents the ligand in CuO) with the combination of a satellite peak (in higher binding energy) containing $d^9$ character. In case of $Cu_2O$, which have a filled ground state ($d^{10}$) configuration, such a transition is not possible and would not result in the satellite peak.[19,46] Also core level spectrum for O 1s (Figure S3b in Supporting Information) confirms the formation of Cu—O bonds associated with CuO.[41,44,45]

Both XPS and FTIR results are consistent with TEM measurements.

The mechanisms leading to the formation of CuO NPs will be now discussed. The investigation of mechanisms induced at the plasma-liquid interface represents a new and fast growing field within the plasma community.[31,33,47–51] Despite much recent progress, many aspects that can lead to a description of this non-equilibrium and complex interface are still under debate. Nonetheless, hybrid plasma-liquid systems are producing important contributions to nanomaterial synthesis and surface treatment.[31,33,47,50,52–57] In particular, hybrid plasma-liquid approaches have been used to produce various Cu and Cu-oxide nanostructures, often leading to mixed phases.[39,54,58,59] In all these cases, the synthesis conditions have differed dramatically in terms of precursors, solution compositions, and plasma configurations/coupling. For instance, solutions have been made in some cases by adding the $K_2CO_3$ or citrate buffer or NaCl in water.[54,59] Super dehydrated ethanol was also employed as an electrolyte

for etching the copper electrode[39] under argon gas atmosphere and resulted in $Cu_2O/CuO$-carbon nanocomposites. Plasmas generated at the surface or within the solution have been used, drastically changing the impact of physical and chemical phenomena. Therefore, it is difficult to extract meaningful comparisons from such diverse conditions. Our synthesis method takes advantage of the simple chemistry with very few components (only a copper electrode and ethanol) and benefits from plasma-based reduction, leading to pure CuO NPs. With the current knowledge of plasma liquid-interactions we are therefore able to discuss the mechanisms leading to the formation of the CuO NPs according to the following reactions:

$$Cu^{(0)} \rightarrow Cu^{1+} + e^- \qquad (1)$$

$$Cu^{1+} + e^-_{(solvated)} \rightarrow Cu^{(0)} \qquad (2)$$

$$Cu^{(0)} + H_2O_2 \rightarrow CuO + H_2O \qquad (3)$$

The first reaction is the result of passive anodic dissolution as expected due to the applied current,[60] where the resulting electron closes the current loop into the copper electrode. Anodic dissolution can also result in Cu-ions with oxidation state of 2. Reduction of Cu-ions, from an oxidation state of 1 or 2 to $Cu^{(0)}$, however, does not take place as in standard electrochemical cells due to the absence of a solid counter-electrode. On the contrary, at the plasma-liquid interface, solvated electrons[51] act as reducing agent producing atomic $Cu^{(0)}$, equation (2). The plasma-ethanol interface is also known to produce radicals leading to the formation of hydrogen peroxide ($H_2O_2$)[52,53,61] and we have confirmed that also in our case $H_2O_2$ is produced and consumed by equation (3) (see Supporting Information).[62] The interaction of locally produced (i.e., close to the interface) $H_2O_2$ with reduced copper atoms then leads to the formation of CuO,[63,64] where the very high reaction rates of solvated electrons and the non-acidic state (>6 pH; measured before and after synthesis, see Supporting Information) prevents Fenton-like reactions with the Cu-ions.[51,65] The size of the NPs is then determined by the local concentration of coalescing CuO. Absence and delays of oxidation through equation (3) would otherwise cause the growth of larger size particles.[56] We, therefore, believe that the small reaction volume close to the plasma-liquid interface, where the concentration of solvated electrons is high, is responsible for the small size and narrow size distribution of the NPs. As reduction takes place in this small volume, NPs that are formed and oxidized here are prevented from growing or oxidizing any further as they move out of the "reaction volume" due to either diffusion or circulating currents imposed by the plasma gas flow. Finally, because oxidation takes place only through reaction (2) in this highly reactive volume, only pure phase CuO NPs are produced.

We have then investigated important properties of the CuO NPs in order to provide useful information for their use in a range of energy-relevant applications. We have performed transmission and reflectance measurements, which offered the possibility to determine the direct bandgap of the NPs.[30] Ultraviolet-visible (UV-Vis) transmission and reflectance measurements were carried out with a deuterium-halogen lamp (Ocean Optics DH-2000-BAL) as light source and an integrating sphere (Ocean Optics ISP-50-8-R-GT). In this case, CuO NPs were spray-coated on quartz substrates and dried. The extrapolated value of the direct bandgap is 2.9 eV (see Figures 3c and S5, Supporting Information), which is much larger than the bulk bandgap (1.2 eV).[13,16] The widening of the bandgap is expected when the radius of the CuO NPs approaches the exciton-Bohr radius.[21,30] In Figure 3d, we report the trend of the bandgap widening with the decreasing diameter. The reported data points refer to the bandgap value determined for the CuO NPs (blue circle), having a measured diameter around 1.9 nm, and the ones reported in the literature for larger CuO nanoparticles (black squares), characterized by larger diameters,[18,66] which confirm the expected trend with decreasing diameter. The bulk bandgap is also reported for comparison.

In order to determine the Fermi level ($E_f$) of the CuO NPs by Kelvin probe measurements (SKP Kelvin Probe Version Delta 5+, Version 5.05 from KP Technology Ltd., UK), colloids were spray-coated on glass substrates coated with indium-tin-oxide (ITO). Kelvin probe measurements produced a Fermi level of −5.37 eV (Figure S4, Supporting Information), in agreement with previously reported levels.[67] The valence band-edge value of −6.3 eV has been determined from ultra-violet photoemission spectroscopy (UPS) measurements (Figure S6, Supporting Information). UPS was carried out with a KRATOS Axis Ultra DLD spectrometer and measurements were taken at $>2 \times 10^{-8}$ mbar base pressure and He I ($h = 21.22$ eV) as the excitation source. Samples were prepared by spray coating the CuO NPs on ITO-coated glass. The conduction band edge is then determined by adding the bandgap to the valence band-edge, which results into −3.4 eV. These measurements (i.e., by UV-Vis, Kelvin probe, and UPS) have allowed for the estimation of the EBD, see inset of Figure 3d. The determination of the EBD represents a fundamental step toward the application of CuO NPs for photovoltaic and other energy devices.

The study and measurement of the EBD of our CuO NPs has revealed the conditions for optimal band alignment with a type of third generation devices. In particular, the p-type nature, wide bandgap and high conduction band-edge, makes CuO NPs highly suitable to be integrated in devices where an electron blocking layer is required. To demonstrate this principle, we have integrated CuO NPs in an all-inorganic third generation device, which has potential application in
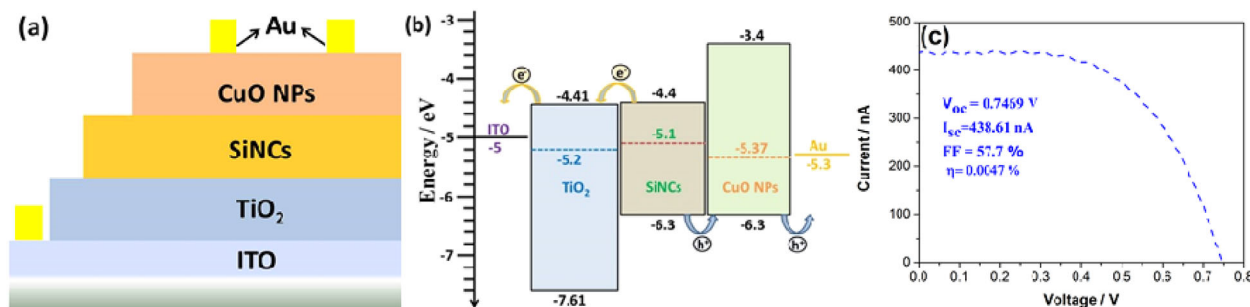
**FIGURE 4** Schematic representation of (a) device structure and (b) corresponding band alignment of the solar cell device; (c) typical current-voltage characteristic of the fabricated devices

multi-junction architectures (absorption of high energy photons) and/or to exploit carrier multiplication. Full fabrication details of the solar cell devices used to demonstrate CuO NPs as an electron blocking layer are reported in the Supporting Information.

The device structure and corresponding non-equilibrated energy level diagram is illustrated in Figure 4a and b, respectively. Current voltage (*I-V*) graph of our best device is shown in Figure 4c, which clearly shows the efficacy of the CuO NPs in reducing interface carrier recombination, providing good rectification, a relatively high fill factor (58%), and very high open-circuit voltage (0.75 V); average values for a series of devices can be found in the Supporting Information (Figure S7). In particular, the open-circuit voltage ($V_{oc}$) represents the highest value produced for inorganic devices with Si NCs, which is a result of the alignment with the CuO NPs layer; devices produced without the CuO NP layer resulted in shunting. Our quantum confined CuO NPs exhibit a lower conduction/higher valence band-edge than other selective transport layers reported in the literature,[67–71] which largely favors separation of carriers. A full comparison with relevant and equivalent devices is reported in Tables S1 and S2 in Supporting Information.

At this time, the device is not fully optimized and further work will be reported demonstrating the impact of tailoring the different device components and fabrication steps. As a consequence the short-circuit current is very low (439 nA), which is the main reason for an overall low device efficiency (0.005%).

Nonetheless, this represents the first example of an all-inorganic device based on Si NCs as active layer and fully demonstrates the functionality of the CuO NPs. A key role is played here by the band alignment where quantum confinement effect has allowed to up-shift the conduction band-edge of the CuO NPs with respect to the Si NCs, yet preserving hole conduction from the Si NCs through the CuO NPs and to the Au contact. Furthermore, the Fermi level is also well aligned with Si NCs so to promote suitable band-bending at the Si-CuO interface for hole dissociation and transport into the CuO NPs layer.

## 4 | CONCLUSION

In summary, we have demonstrated that high quality and high purity ultra small and quantum confined CuO NPs can be rapidly synthesized with a simple and environmentally friendly one-step synthesis method. The synthesized CuO NPs show quantum confined properties, which suggest the possibility of using Cu-based oxide for different applications and importantly with size-dependent functions in solar cell devices through appropriate EBD-engineering. In addition to essential material properties, we have also produced important information on the energy structure of the NPs, required to evaluate their suitability in application devices. We have, therefore, demonstrated the possibility of using CuO NPs as an effective electron blocking layer in all-inorganic, green, third generation devices.

### REFERENCES

[1] A. H. MacDonald, *Nature* **2001**, *414*, 409.

[2] C. L. Hsin, J. H. He, C. Y. Lee, W. W. Wu, P. H. Yeh, L. J. Chen, Z. L. Wang, *Nano Lett.* **2007**, *7*, 1799.

[3] P. M. Rao, X. Zheng, *Nano Lett.* **2009**, *9*, 3001.

[4] D. P. Puzzo, M. G. Helander, P. G. O'Brien, Z. Wang, N. Soheilnia, N. Kherani, Z. Lu, G. A. Ozin, *Nano Lett.* **2011**, *11*, 1457.

[5] J. Gao, C. L. Perkins, J. M. Luther, M. C. Hanna, H.-Y. Chen, O. E. Semonin, A. J. Nozik, R. J. Ellingson, M. C. Beard, *Nano Lett.* **2011**, *11*, 3263.

[6] D. Cao, C. Wang, F. Zheng, W. Dong, L. Fang, M. Shen, *Nano Lett.* **2012**, *12*, 2803.

[7] R. S. Devan, R. A. Patil, J. H. Lin, Y. R. Ma, *Adv. Funct. Mater.* **2012**, *22*, 3326.

[8] G. Hautier, A. Miglio, G. Ceder, G.-M. Rignanese, X. Gonze, *Nat. Commun.* **2013**, *4*, 2292.

[9] Y. N. Ko, S. Bin Park, K. Y. Jung, Y. C. Kang, *Nano Lett.* **2013**, *13*, 5462.

[10] F. Fu, T. Feurer, T. Jäger, E. Avancini, B. Bissig, S. Yoon, S. Buecheler, A. N. Tiwari, *Nat. Commun.* **2015**, *6*, 8932.

[11] M. T. Greiner, M. G. Helander, W.-M. Tang, Z.-B. Wang, J. Qiu, Z.-H. Lu, *Nat. Mater.* **2012**, *11*, 76.

[12] Z. Bian, T. Tachikawa, P. Zhang, M. Fujitsuka, T. Majima, *Nat. Commun.* **2014**, *5*, 3038.

[13] B. Balamurugan, B. R. Mehta, *Thin Solid Films* **2001**, *396*, 90.

[14] X. Jiang, T. Herricks, Y. Xia, *Nano Lett.* **2002**, *2*, 1333.

[15] Y. Feng, X. Zheng, *Nano Lett.* **2010**, *10*, 4762.

[16] M. U. Anu Prathap, B. Kaur, R. Srivastava, *J. Colloid Interface Sci* **2012**, *370*, 144.

[17] W. Wang, L. Wang, H. Shi, Y. Liang, *CrystEngComm* **2012**, *14*, 5914.

[18] C. Yang, F. Xiao, J. Wang, X. Su, *J. Colloid Interface Sci.* **2014**, *435*, 34.

[19] K. Borgohain, J. Singh, M. Rama Rao, T. Shripathi, S. Mahamuni, *Phys. Rev. B* **2000**, *61*, 11093.

[20] Y. Xu, D. Chen, X. Jiao, *J. Phys. Chem. B* **2005**, *109*, 13561.

[21] S. P. Meshram, P. V. Adhyapak, U. P. Mulik, D. P. Amalnerkar, *Chem. Eng. J.* **2012**, *204–205*, 158.

[22] O. Langmar, C. R. Ganivet, A. Lennert, R. D. Costa, G. de la Torre, T. Torres, D. M. Guldi, *Angew. Chemie Int. Ed.* **2015**, *54*, 7688.

[23] Q. Zhang, K. Zhang, D. Xu, G. Yang, H. Huang, F. Nie, C. Liu, S. Yang, *Prog. Mater. Sci.* **2014**, *60*, 208.

[24] A. S. Zoolfakar, R. A. Rani, A. J. Morfa, A. P. O'Mullane, K. Kalantar-zadeh, *J. Mater. Chem. C* **2014**, *2*, 5247.

[25] Q. Zhang, D. Xu, X. Zhou, X. Wu, K. Zhang, *Small* **2014**, *10*, 935.

[26] H. He, J. Dong, K. Li, M. Zhou, W. Xia, X. Shen, J. Han, X. Zeng, W. Cai, *RSC Adv.* **2015**, *5*, 19479.

[27] E. Thimsen, M. Johnson, X. Zhang, A. J. Wagner, K. A. Mkhoyan, U. R. Kortshagen, E. S. Aydil, *Nat. Commun.* **2014**, *5*, 5822.

[28] M. Bouchard, M. Létourneau, C. Sarra-Bournet, M. Laprise-Pelletier, S. Turgeon, P. Chevallier, J. Lagueux, G. Laroche, M.-A. A. Fortin, *Langmuir* **2015**, *31*, 7633.

[29] C. Jin, M. Hu, X. Cheng, F. Bu, L. Xu, Q. Zhang, J. Jiang, *Chem. Commun.* **2015**, *51*, 206.

[30] S. Dagher, Y. Haik, A. I. Ayesh, N. Tit, *J. Lumin.* **2014**, *151*, 149.

[31] C. Richmonds, R. M. Sankaran, *Appl. Phys. Lett.* **2008**, *93*, 131501.

[32] A. Kumar, P. Ann Lin, A. Xue, B. Hao, Y. Khin Yap, R. M. Sankaran, *Nat. Commun.* **2013**, *4*, 2618.

[33] T. Yan, X. Zhong, A. E. Rider, Y. Lu, S. A. Furman, K. (Ken) Ostrikov, *Chem. Commun.* **2014**, *50*, 3144.

[34] C. Du, M. Xiao, *Sci. Rep.* **2014**, *4*, 7339.

[35] V. Švrček, D. Mariotti, M. Kondo, *Appl. Phys. Lett.* **2010**, *97*, 161502.

[36] V. Svrcek, K. Dohnalova, D. Mariotti, M. T. Trinh, R. Limpens, S. Mitra, T. Gregorkiewicz, K. Matsubara, M. Kondo, *Adv. Funct. Mater.* **2013**, *23*, 6051.

[37] V. Svrcek, D. Mariotti, S. Mitra, T. Kaneko, L. Li, U. Cvelbar, K. Matsubara, M. Kondo, *J. Phys. Chem. C* **2013**, *117*, 10939.

[38] W. Jia, Y. Liu, P. Hu, R. Yu, Y. Wang, L. Ma, D. Wang, Y. Li, *Chem. Commun.* **2015**, *51*, 8817.

[39] D. S. Kozak, R. A. Sergiienko, E. Shibata, A. Iizuka, T. Nakamura, *Sci. Rep.* **2016**, *6*, 21178.

[40] M. Huang, Y. Zhang, F. Li, Z. Wang, Alamusi, N. Hu, Z. Wen, Q. Liu, *Sci. Rep* **2014**, *4*, 4518.

[41] S. Sun, X. Zhang, Y. Sun, S. Yang, X. Song, Z. Yang, *Phys. Chem. Chem. Phys.* **2013**, *15*, 10904.

[42] Y. Shen, M. Guo, G. Shao, *Acta Mater.* **2015**, *85*, 122.

[43] M. C. Biesinger, L. W. M. Lau, A. R. Gerson, R. S. C. Smart, *Appl. Surf. Sci.* **2010**, *257*, 887.

[44] P. Gao, Y. Gong, N. P. Mellott, D. Liu, *Electrochim. Acta* **2015**, *173*, 31.

[45] Y. Ge, Z. H. Shah, C. Wang, J. Wang, W. Mao, S. Zhang, R. Lu, *ACS Appl. Mater. Interfaces* **2015**, *7*, 26437.

[46] J. Hernandez, P. Wrschka, G. S. Oehrlein, *J. Electrochem. Soc.* **2001**, *148*, G389.

[47] D. Mariotti, R. M. Sankaran, *J. Phys. D. Appl. Phys.* **2011**, *44*, 174023.

[48] D. Mariotti, J. Patel, V. Svrcek, P. Maguire, *Plasma Process. Polym.* **2012**, *9*, 1074.

[49] D. Zhu, L. Zhang, R. E. Ruther, R. J. Hamers, *Nat. Mater.* **2013**, *12*, 836.

[50] P. Rumbach, M. Witzke, R. M. Sankaran, D. B. Go, *J. Am. Chem. Soc.* **2013**, *135*, 16264.

[51] P. Rumbach, D. M. Bartels, R. M. Sankaran, D. B. Go, *Nat. Commun.* **2015**, *6*, 7248.

[52] D. Mariotti, V. Svrcek, J. W. J. Hamilton, M. Schmidt, M. Kondo, *Adv. Funct. Mater.* **2012**, *22*, 954.

[53] J. Patel, L. Němcová, P. Maguire, W. G. Graham, D. Mariotti, *Nanotechnology* **2013**, *24*, 245604.

[54] X. Hu, X. Zhang, X. Shen, H. Li, O. Takai, N. Saito, *Plasma Chem. Plasma Process.* **2014**, *34*, 1129.

[55] V. Svrcek, T. Yamanari, D. Mariotti, S. Mitra, T. Velusamy, K. Matsubara, *Nanoscale* **2015**, *7*, 11566.

[56] Y. Lu, Z. Ren, H. Yuan, Z. Wang, B. Yu, J. Chen, *RSC Adv.* **2015**, *5*, 62619.

[57] T. Velusamy, S. Mitra, M. Macias-Montero, V. Svrcek, D. Mariotti, *ACS Appl. Mater. Interfaces* **2015**, *7*, 28207.

[58] G. Ren, D. Hu, E. W. C. Cheng, M. A. Vargas-Reus, P. Reip, R. P. Allaker, *Int. J. Antimicrob. Agents* **2009**, *33*, 587.

[59] G. Saito, S. Hosokai, M. Tsubota, T. Akiyama, *J. Appl. Phys.* **2011**, *110*, 23302.

[60] M. Datta, *IBM J. Res. Dev.* **1993**, *37*, 207.

[61] S. Mitra, V. Švrček, D. Mariotti, T. Velusamy, K. Matsubara, M. Kondo, *Plasma Process. Polym.* **2014**, *11*, 158.

[62] E. Vyhnánková, Z. Kozáková, F. Krčma, A. Hrdlička, *Open Chem.* **2014**, *13*, 218.

[63] S. Pandija, D. Roy, S. V. Babu, *Mater. Chem. Phys.* **2007**, *102*, 144.

[64] P. Pootawang, N. Saito, S. Y. Lee, *Nanotechnology* **2013**, *24*, 55604.

[65] M. C. Kang, H.-S. Nam, H. Y. Won, S. Jeong, H. Jeong, J. J. Kim, *Electrochem. Solid-State Lett.* **2008**, *11*, H32.

[66] J. Liu, X. Huang, Y. Li, K. M. Sulieman, X. He, F. Sun, *Cryst. Growth Des.* **2006**, *6*, 1690.

[67] Q. Xu, F. Wang, Z. Z. Tan, L. Li, S. Li, X. Hou, G. Sun, X. Tu, J. Hou, Y. Li, *ACS Appl. Mater. Interfaces* **2013**, *5*, 10658.

[68] H.-T. Lien, D. P. Wong, N.-H. Tsao, C.-I. Huang, C. Su, K.-H. Chen, L.-C. Chen, *ACS Appl. Mater. Interfaces* **2014**, *6*, 22445.

[69] C. Zuo, L. Ding, *Small* **2015**, *11*, 5528.

[70] J. Zhang, J. Wang, Y. Fu, B. Zhang, Z. Xie, *RSC Adv.* **2015**, *5*, 28786.

[71] Z. Yu, W. Liu, W. Fu, Z. Zhang, W. Yang, S. Wang, H. Li, M. Xu, H. Chen, *J. Mater. Chem. A* **2016**, *4*, 5130.

## SUPPORTING INFORMATION

Additional Supporting Information may be found online in the supporting information tab for this article.

**How to cite this article:** Velusamy T, Liguori A, Macias-Montero M, et al. Ultra-small CuO nanoparticles with tailored energy-band diagram synthesized by a hybrid plasma-liquid process. *Plasma Process Polym*. 2017;e1600224, https://doi.org/10.1002/ppap.201600224